Heliyon 10 (2024) e23218

Contents lists available at ScienceDirect

Heliyon

journal homepage: www.cell.com/heliyon

The engineering, drug release, and *in vitro* evaluations of the PLLA/HPC/*Calendula Officinalis* electrospun nanofibers optimized by Response Surface Methodology

Pegah Momeni [a], Maryam Nourisefat [b], Arman Farzaneh [b], Mohammad Shahrousvand [c,*], Mohammad Hossein Abdi [d]

[a] *Faculty of Polymer Engineering, Sahand University of Technology, Tabriz, Iran*
[b] *Department of polymer engineering and color technology, Amirkabir University of Technology, Tehran, Iran*
[c] *Caspian Faculty of Engineering, College of Engineering, University of Tehran, Rezvanshahr, P.O. Box: 43841-119, Guilan, Iran*
[d] *School of Chemical and polymer Engineering, College of Engineering, University of Tehran, Tehran, Iran*

ARTICLE INFO

Keywords:
Poly (L-lactic acid) (PLLA)
Hydroxypropyl cellulose (HPC)
Electrospun nanofibers
Response surface methodology (RSM)
Calendula Officinalis (*marigold*) extract
Biomedical applications

ABSTRACT

A system based on poly(L-lactic acid) (PLLA) and hydroxypropyl cellulose (HPC) was considered in this study to achieve electrospun mats with outstanding properties and applicability in biomedical engineering. A novel binary solvent system of chloroform/N,N-dimethylformamide (CF/DMF:70/30) was utilized to minimize the probable phase separation between the polymeric components. Moreover, Response Surface Methodology (RSM) was employed to model/optimize the process. Finally, to scrutinize the ability of the complex in terms of drug delivery, Calendula Officinalis (Marigold) extract was added to the solution of the optimal sample (Opt.PH), and then the set was electrospun (PHM). As a result, the presence of Marigold led to higher values of fiber diameter (262 ± 34 nm), pore size (483 ± 102 nm), and surface porosity (81.0 ± 7.3 %). As this drug could also prohibit the micro-scale phase separation, the PHM touched superior tensile strength and Young modulus of 11.3 ± 1.1 and 91.2 ± 4.2 MPa, respectively. Additionally, the cumulative release data demonstrated non-Fickian diffusion with the Korsmeyer-Peppas exponent and diffusion coefficient of n = 0.69 and D = 2.073 × 10^{-14} cm^2/s, respectively. At the end stage, both the Opt.PH and PHM mats manifested satisfactory results regarding the hydrophilicity and cell viability/proliferation assessments, reflecting their high potential to be used in regenerative medicine applications.

1. Introduction

Polymers, drugs, mineral nanoparticles, and functional agents are among the materials repeatedly used to form electrospun scaffolds applicable in diverse situations, such as in wound regeneration, bone repair, retinal transplantation, and cancer treatment [1, 2]. Regarding the polymeric components, poly(ε-caprolactone) (PCL), polyacrylic acid (PAA), polyethylene oxide, polyurethanes, and poly(L-lactic acid) (PLLA) are well-known synthetic materials with appropriate biodegradability, biocompatibility, processability, and mechanical properties [3–8]. Although the hydrophobicity of a large number of these polymers challenges their biomedical

* Corresponding author.
E-mail address: mohammadshahrousvand@yahoo.com (M. Shahrousvand).

https://doi.org/10.1016/j.heliyon.2023.e23218
Received 24 August 2023; Received in revised form 28 November 2023; Accepted 29 November 2023
Available online 3 December 2023

application, the addition of natural polymers, including chitosan, gelatin, collagen, xanthan gum, and cellulose derivatives, would cover such a disadvantageous aspect. This combination of components would also negate the weak mechanical properties of natural polymers [9–12]. Additionally, in drug delivery cases, some natural polymers such as hydroxypropyl cellulose (HPC) may act as drug stabilizers and promote release performance in the early and/or end stage [13–15].

Meanwhile, PLLA, as a synthetic, semi-crystalline, and biodegradable aliphatic polyester with desirable biocompatibility, tensile strength, and Young modulus, has enticed an increasing attention for biomedical applications. In a comparative study, Wulf et al. showed that PLLA in both film and fiber forms has dual drug delivery capability for Paclitaxel (PTX) and growth factor VEGF. They illustrated that thank to the higher specific surface in the obtained electrospun mats, higher amounts of drug could be loaded. Hence, the cumulative release from fibers during 70 days was three times higher than that in the film state [16]. Rashidi et al. also prepared core-shell fibers of PLLA/gelatin with a mean diameter of 348 nm. They manifested that the prepared system has higher mechanical properties than that of each single component. In addition, it was reported that due to the presence of gelatin, degradation of final mat occurs in a short period of 11 days [17].

Notably, PLLA faces some restrictions concerning its poor miscibility with the numerous polar/natural polymers. In other words, the considerable phase separation potency of PLLA has placed it in a challenging state regarding the electrospinning of its blend solutions. Moreover, the non-availability of suitable joint solvents for PLLA and some widely used natural polymers is another issue that exacerbates such process limitations [18–20]. These conditions have caused the electrospinning of PLLA and its blends to be highly sensitive to the parameters involved in this process, including system concentration, applied voltage, flow rate, and electrospinning distance. Therefore, aiming to reach the optimal levels of the parameters as well as the least morphological and structural defects in the final fibers, it is necessary to consider a comprehensive design logic in addition to selecting an appropriate solvent system [21–24].

Response Surface Methodology (RSM) is an efficacious and systematic approach to the design of experiments (DoE) and modeling/optimizing a wide range of processes. Unlike the traditional methods, this approach can investigate the effect of simultaneous changes in several variables and monitor their interaction with each other [25,26]. Jadbabaei et al. nicely applied the RSM to prepare a potential electrospun scaffold based on polyvinyl alcohol/sodium alginate. Alongside the detailed explanations of DoE outcomes, they have clarified that the optimized scaffolds revealed appropriate degradation rate, swelling behavior, mechanical properties, and cell biocompatibility [27]. Guerreiro et al. designed a blend electrospun mat based on PCL/gelatin, which could release protein for skin repair applications. However, their study did not investigate the effect of this design/optimization on physical and mechanical properties. Also, the optimal sample was not validated based on rheological and physicochemical principles [28]. Remarkably, DoE is not only specific to the electrospinning process and is also operative in other techniques. In this regard, Behravesh et al. optimized the synthesis of PAA/gum Arabic/zinc oxide hydrogels based on RSM and compared the morphological and swelling properties of the samples. They exhibited that the final predicted models reasonably agreed with the logic and principles of polymerization [29].

Thus, relying on the RSM and using a novel solvent system, a set based on PLLA associated with HPC was precisely designed and electrospun in the present research. Notably, the Central Composite Design (CCD) approach was considered while employing the RSM. Compared to the Box Benken Design (BBD) that allows each variable to vary in only three levels, the CCD provides five levels for the variation of variables. This causes more experiments to be examined in the CCD approach, which would result in more accurate and reliable modeling/optimization. Following the modeling and optimization stage, the accuracy of the suggested optimal sample was also investigated using physicochemical relationships. Next, a single dose of *Calendula Officinalis (Marigold)* hydroethanolic extract was added to the optimal PLLA/HPC sample. Encompassing amino acids, fatty acids, hydroxycoumarin, and flavonoids (quercetin and isorhamnetin) led this extract to have considerable potential in inflammation reduction, angiogenesis, and wound healing. Hence, *Marigold* has been frequently utilized in fabricating wound dressings [30–32]. The presence of this drug in this work aims to track its release behavior/kinetic in a new polymer matrix and provides a basis for further research. Eventually, the optimal PLLA/HPC and drug-loaded samples were subjected to engineering and *in vitro* evaluations/comparisons. It should be noted that based on the authors' best knowledge and according to the present materials set, this study algorithm has yet to be detailed in the literature so far.

2. Materials and methods

2.1. Materials

PLLA (4023D) (220 $kg.mol^{-1}$) was supplied by NatureWorks Company. HPC (160 $kg.mol^{-1}$), tetrazolium salt 3-(4,5 dimethylthiazol-2-yl)-2,5-diphenyl tetrazolium bromide (MTT), and acridine orange (AO) stain were provided from Sigma-Aldrich. Chloroform (CF) and N,N-dimethylformamide (DMF) were purchased from Merck. *Marigold* extract and Phosphate buffered saline tablets (PBS, pH = 7.4) were also prepared from Gol-Sanam and GIBCO Companies, respectively. Eventually, the L929 fibroblast cells were obtained from the Histogenetic Cell and Animal Research Center. All the materials were utilized with no more purification or modification.

2.2. Providing the DoE table for PLLA/HPC systems

According to the RSM fundamentals and based on the literature, the variables (factors), their range of diversity, as well as the responses were defined in the first step. In this respect, the most determinative structural and process parameters, i.e., the concentration of polymeric components (PLLA and HPC) and electrospinning distance, were considered as factors. The range of factors included PLLA Conc.: [5 to 14] wt./v %, HPC Conc.: [2 to 8] wt./v %, and electrospinning distance: [10 to 20] cm. The logic of selecting

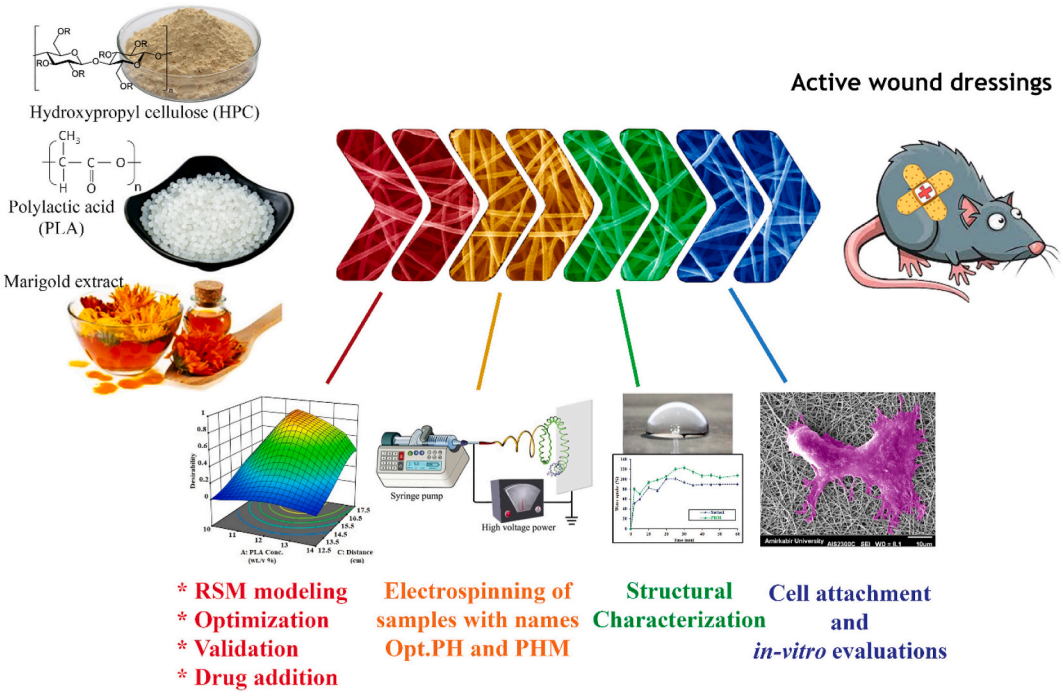

Fig. 1. An overview of the steps and principles implemented in this research.

these ranges was based on the frequent concentrations applied in the previous studies of researchers. Eventually, the average fiber diameter, fiber diameter distribution, and the number of defects (beads) in the fibers were considered as responses to track the behavior/effect of the factors. Table S1 exhibits the actual levels of the factors, which were combined into 20 runs via the *Design Expert* software (V11.1.2.0).

After executing the DoE runs, all the responses of each run were measured according to the scanning electron microscopy (SEM) (AIS2100, Seron Technology, South Korea) micrographs and entered into the software. Notably, Meyerhoff equations were used to calculate the fiber diameter distribution (**Eq. S1**, **S2**, and **S3**). Next, regarding the modeling phase, **Eq. (1)** was considered to describe each response in terms of the above-defined factors. Based on the fundamentals of RSM, this equation is allowed only to form an interactive first-order (2FI) or quadratic polynomial function. The validation and significance of the models were evaluated by ANOVA statistical protocol (by *design expert* software). In this equation, Y represents the response (output) studied in the research. β_0 is the numerical value of the response when all the factors are at the center point of their defined levels. β_i, β_{ij}, and β_{ii} are coefficients for linear, interactive, and quadratic sentences, respectively. Also, X_i and X_j represent the factors (inputs) in the suggested model [26].

$$Y = \beta_0 + \sum_{i=1}^{4} \beta_i X_i + \sum_{i=1}^{3} \sum_{j=i+1}^{4} \beta_{ij} X_i X_j + \sum_{i=1}^{4} \beta_{ii} X_i^2 \quad (1)$$

2.3. DoE optimization and physicochemical validation of optimal PLLA/HPC sample

In the RSM optimization stage, minimizing all the responses was aimed at obtaining fibers with the highest uniformity and the lowest mean diameter. Achieving this goal could ensure that even if the other components (e.g., drugs) are added to the system, the morphological properties of the fibers do not undergo a drastic change and remains within an acceptable range. Simply put, this optimization acted as a safety factor.

The optimal sample was also evaluated from the physicochemical viewpoint to verify the optimization results. Based on this perspective, the chain entanglement density (β) of the optimal PLLA/HPC solution was calculated according to **Eq. (2)**. This relationship is counted as a criterion for the spinnability of the polymeric solutions, where $\beta \geq 3.5$ denotes the formation of flawless fibers [33]. In this equation, $\overline{M_w}$, φ_c, and $\overline{M_e}$ are the average molecular weight, concentration, and entanglement molecular weight of the polymers [34].

$$\beta = \frac{\overline{M_w} \times \varphi_c}{\overline{M_e}} \quad (2)$$

2.4. Obtaining marigold-loaded PLLA/HPC sample

A single dose (10 mg/ml) of *Marigold* was added to the solution of the optimal sample, and the set was subjected to electrospinning. Such a drug level was according to Doostan et al.'s research for electrospun wound dressing preparation [35]. Finally, the optimal and drug-loaded samples were investigated in respect of engineering and *in vitro* analyses (Fig. 1). For simplicity, the PLA/HPC-based samples obtained from the DoE, the optimal one, and the drug-loaded sample are called PH, Opt.PH, and PHM, respectively.

2.5. Preparation of the solutions and detailing the electrospinning procedure

The mixture of CF and DMF was considered a novel binary solvent system for all the solutions. Additionally, the mixing ratio 70:30 (CF:DMF) was selected experimentally to achieve the complete dissolution of polymeric components and, ultimately, a stable electrospinning process (according to the fiber uniformity evaluations detailed in the Supplementary Materials, Fig. S1). Next, aim to prepare PH and Opt.PH samples, PLA pellets, and HPC powder were added to the solvent system, and the complex was stirred at 300 rpm for 4 h. Likewise, in the case of the PHM sample, the *Marigold* extract was added to the solvent system concomitantly with the polymeric contents.

In the following, after pouring the solution of each sample into a syringe (10 ml) associated with a blunt-end needle (G21), the set was established in a syringe pump to carry out the electrospinning process. The flow rate was kept constant throughout the experiments at 0.5 ml/h, and the process was performed at room temperature with a relative humidity of 35–45 %. An aluminum foil-wrapped sheet was considered as the collector, as well. Ultimately, in the range of 15–20 kV, the applied voltage was tuned to form a steady Taylor cone and, subsequently, a stable jet stream.

2.6. Analytical characterizations

2.6.1. Determining the viscosity/electrical conductivity of the solutions

Following the optimization and achieving the Opt.PH and PHM samples, the viscosity and electrical conductivity of their solutions were measured using a Brookfield viscometer (RVDV-II + Pro, USA) and conductivity meter (S230-TDS, Mettler Toledo, Switzerland), respectively. The results would clarify the sensitivity of the process to these two quantities and may promote the justifications in further analyses.

2.6.2. Morphology assessment

As a benchmark, the SEM micrographs were utilized to measure the DoE responses (i.e., average fiber diameter, fiber diameter distribution, and the number of beads) in the PH samples. Opt.PH and PHM samples were also subjected to this microscopy to be characterized regarding the morphological aspects. The surface porosity of these two groups was calculated based on **Eq. (3)** and presuming a small thickness of the mats. According to the equation, A_P is attributed to the summation of the pores' surface area, and A_T is the whole surface area shown in the SEM image [36].

$$Surface\ porosity\ (\%) = \left(\frac{A_P}{A_T}\right) \times 100 \tag{3}$$

2.6.3. Chemical identification

In the wavelength range of $700 - 4000\ cm^{-1}$, the Fourier Transform infrared spectroscopy (FTIR) (Equinox 55 FTIR spectrometer) with 100 scans was employed to determine the chemical bands and intermolecular interactions in the Opt.PH and PHM electrospun mats.

2.6.4. Analysis of the mechanical properties

The mechanical properties of the Opt.PH and PHM samples were investigated in accordance with ASTM D882–10 standard and using a unidirectional tensile device (5566-Applied Science Co., Ithaca, NY). At room temperature and with five times of replication, the specimens with an average thickness of 157 ± 13 μm and rectangular dimensions of $25 \times 5\ mm^2$ were analyzed at the 5 mm/min extension rate.

2.6.5. Hydrophilicity determination

The static sessile drop test was performed to measure the water contact angle (WCA) between the droplet and the surface of the electrospun mats (Opt.PH and PHM). Hence, a drop with a volume of 2 μl was dripped on a $3 \times 3\ cm^2$ piece of mats, and the immediate WCA image was captured by a digital microscope (Dataphysics, OCA15 plus, Germany). Moreover, concerning the PBS absorption level, the Opt.PH and PHM samples were evaluated in a water uptake test (**Eq. (4)**) [37]. Briefly, the dry mats were weighed (W_0) and then dunked in 5 ml PBS under incubation conditions for 24 h at 37 °C). Afterward, the saturated mats were taken out, and prior to re-weighing them (W_1), the leftover water on their surface was removed.

$$Water\ (PBS)\ uptake\ (\%) = \left(\frac{W_1 - W_0}{W_0}\right) \times 100 \tag{4}$$

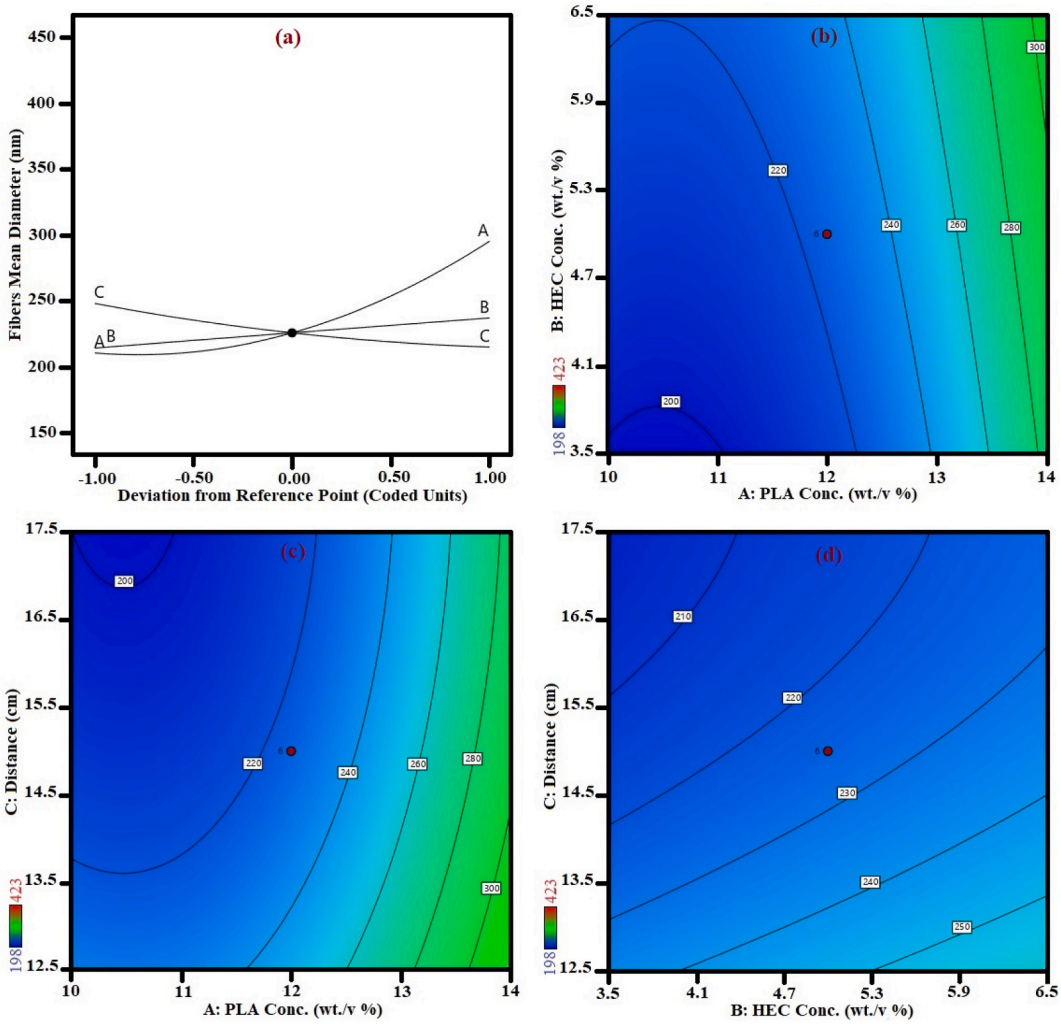

Fig. 2. 1D and 2D diagrams of the first response (Y_1); **(a)** Y_1 vs. deviation from the reference point of each factor; **(b)** Y_1 vs. the simultaneous variation of *A* and *B*; **(c)** Y_1 vs. the simultaneous variation of *A* and *C*; **(d)** Y_1 vs. the simultaneous variation of *B* and *C*.

2.6.6. Cell viability and proliferation

Based on ISO standards 10,993–5:1999, MTT analysis was carried out to quantify the cell viability level of Opt.PH and PHM compared to the control group (TCPS). In detail, UV-sterilized circular samples with a diameter of 1 cm were immersed in a 24-well culture plate containing DMEM/PBS. Then, about 10,000 cells were seeded on the specimen and exposed to 5 % carbon dioxide in an incubator for 3 h at 37 °C. Next, 50 μl of MTT solution was added to wells on days 1, 3, and 5 after cell seeding, and the set was incubated once more. Eventually, the optical density (OD) of the samples was obtained based on the Formazan crystals absorbance at the wavelength of 570 nm (via an ELISA reader (STAT FAX 2100, USA)). In a qualitative appraisal, the cells (cultured for 24 h) on Opt. PH and PHM samples were fixed using glutaraldehyde vapor, and their SEM images were recorded to detect cell attachment/spreading. In Parallel, as a distinguished analysis, cells cultured for 24 h were stained with 1 μl AO to characterize cell compatibility, viability, and proliferation quality via a fluorescent microscope.

2.6.7. Evaluation of the drug release kinetic/mechanism

Aiming to track the *in vitro* release behavior of *Marigold* extract, a 3 × 3 cm^2 piece of PHM mat was immersed in a closed container including 30 ml PBS (at 37 °C). Then, at specific time points, 2 ml of the solution was taken, and its UV absorption was recorded at the wavelength of 250 nm using a UV–vis spectrometer (LAMBDA™ 1050 UV–Vis/near-infrared, PerkinElmer, Waltham, USA). Finally, based on a calibration curve, the absorption data were converted to the cumulative release of the drug, and its graph was plotted. In the following, cumulative release data were fitted in eight models: Zero-order, First-order, Higuchi, Hixson-Crowell, Baker-Lonsdale, Korsmeyer-Peppas, Kopcha-Alfrey, and Gompertz to investigate the release kinetics/mechanism of the *Marigold* extract incorporated in the polymeric matrix (all the models were listed in Table S2). Ultimately the diffusion coefficient (D) in the system was calculated based on **Eq. (5)**, in which d is the average fiber diameter, tan θ denotes the line slope in the plot of M_t/M_0 vs. $t^{1/2}$, and M_0 is the initial

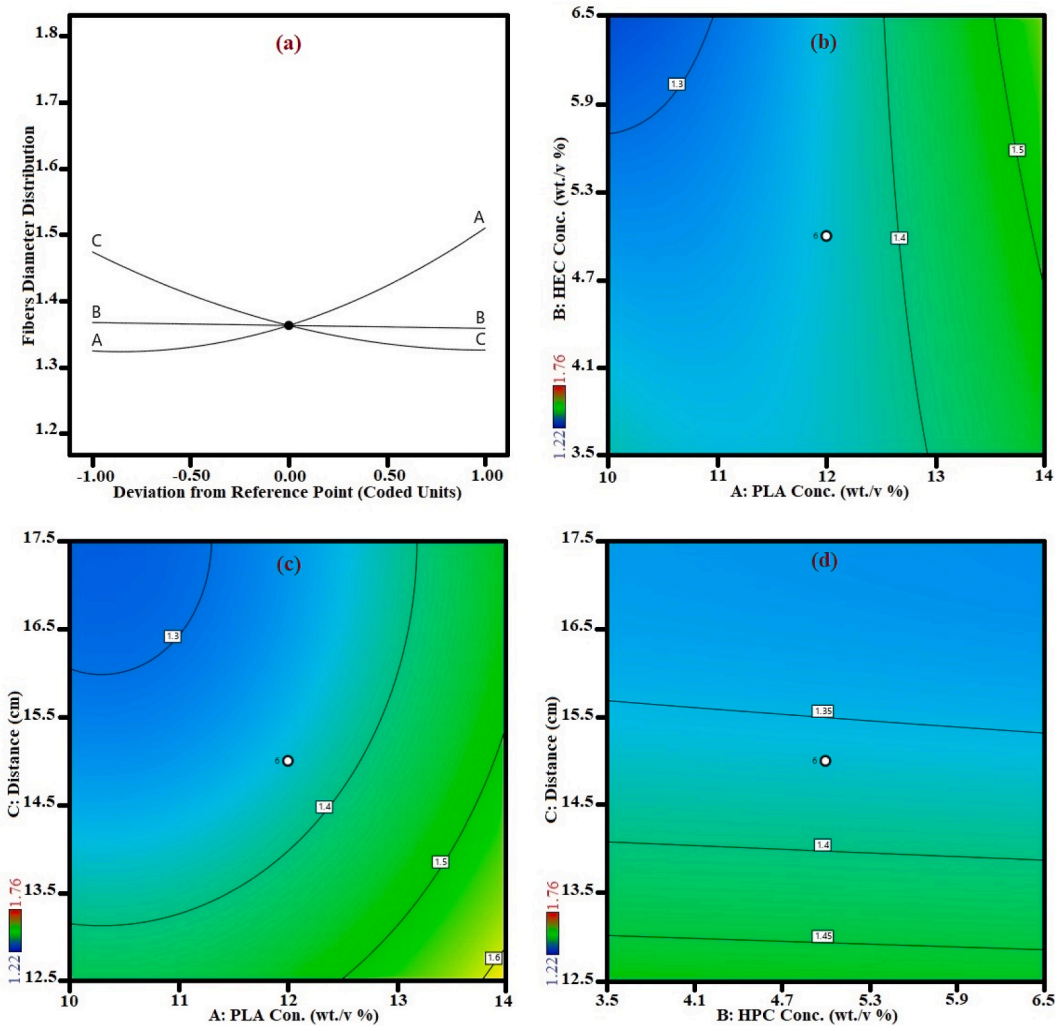

Fig. 3. 1D and 2D diagrams of the second response (Y_2); **(a)** Y_2 vs. deviation from the reference point of each factor; **(b)** Y_2 vs. the simultaneous variation of *A* and *B*; **(c)** Y_2 vs. the simultaneous variation of *A* and *C*; **(d)** Y_2 vs. the simultaneous variation of *B* and *C*.

amount of drug within the mat. Also, M_t is the cumulative amount of the drug released up to the time t [38,39].

$$D = \left(\frac{d(tan\ \theta)}{12M_0}\right)^2 \quad 5$$

2.6.8. Statistical investigation

The DoE data were wholly controlled in terms of the ANOVA section defined in design expert software. The other results reported within the engineering and *in vitro* assessments were obtained after at least three-time replications, and the final average quantities were associated with standard deviation (average ± standard deviation).

3. Results and discussions

3.1. The DoE modeling/optimization

After attaining the SEM photographs of the PH specimens (Fig. S2), the DoE responses were measured in accordance with Table S3. The responses, including Y_1: the average fiber diameter, Y_2: fiber diameter distribution, and Y_3: the number of defects, were then modeled in terms of the factors (*A*: PLLA Conc., *B*: HPC Conc., and *C*: electrospinning distance). Table S4 represents the final equation and statistical information related to the Y_1 model, associated with a high regression coefficient of $R^2 = 0.98$. Fig. 2 (a-d) also discloses 1D and 2D (contour) diagrams describing the dependency of Y_1 to the singular or paired variation of the factors. Based on the mathematical model and the resulted plots, it is predicted that among all the factors, the PLLA concentration will be associated with the

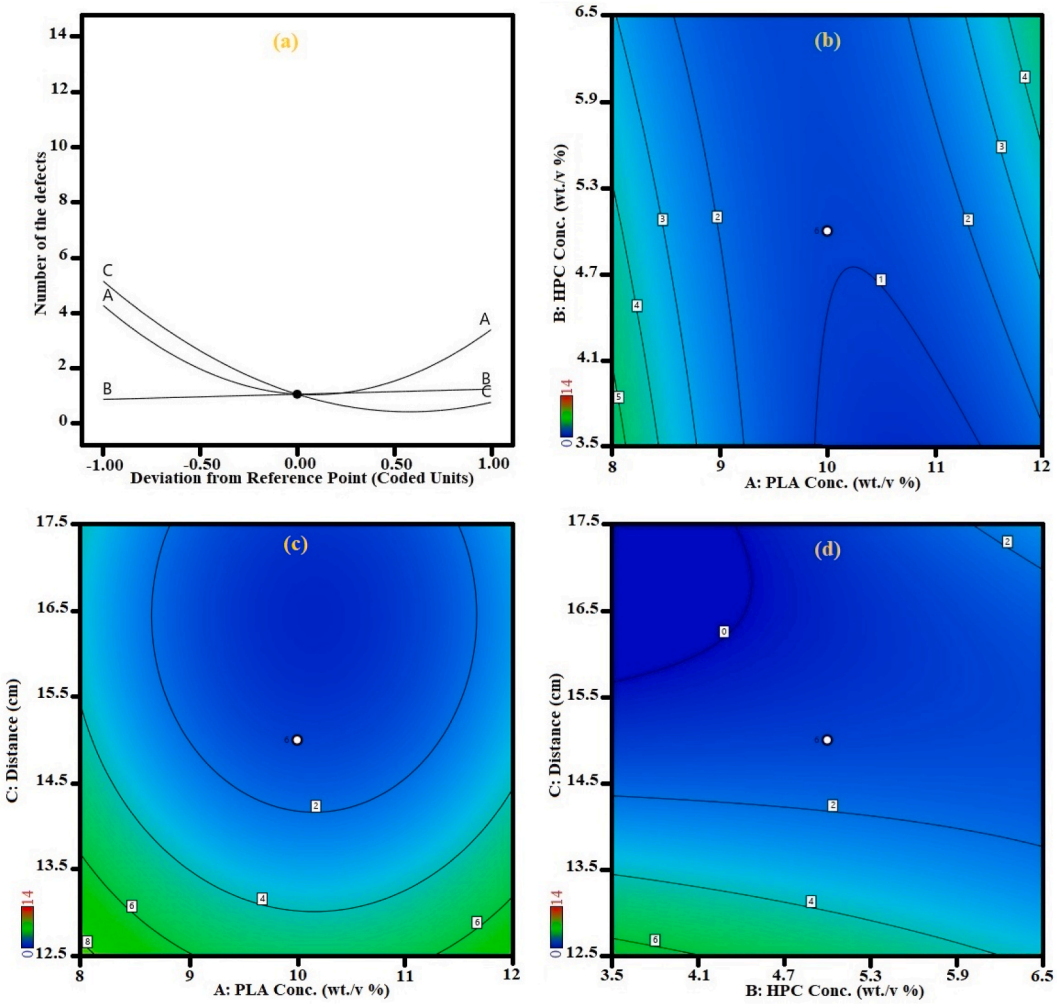

Fig. 4. 1D and 2D diagrams of the third response (Y_3); **(a)** Y_3 vs. deviation from the reference point of each factor; **(b)** Y_3 vs. the simultaneous variation of *A* and *B*; **(c)** Y_3 vs. the simultaneous variation of *A* and *C*; **(d)** Y_3 vs. the simultaneous variation of *B* and *C*.

greatest impact on the average fiber diameter.

According to a modified quadratic function obtained for fiber diameter distribution (Y_2, Table S5), and based on the 1D/2D plots (Fig. 3 (a-d)), it can be concluded that fiber diameter distribution in PH samples would be directly proportional to the PLA concentration and inversely proportional to the electrospinning distance. It is while that the HPC concentration is supposed to have no significant effect on the Y_2.

Eventually, based on the diagrams shown in Fig. 4 (a-d), the increment of PLLA concentration is predicted to result in a dual behavior of Y_3. In other words, increasing this factor up to 12 wt/v % is expected to reduce the number of defects, while exceeding this range would escalate the probability of bead formation. Such behavior can be ascribed to the high viscosity of the PLLA, which may cause an imbalance in the applied forces of the electrospinning process. With these all, it is predicted that enhancing the electrospinning distance would continually reduce the number of defects. Remarkably, all these trends followed a modified quadratic model, which was eventually considered for the third response (Y_3, Table S6).

After the modeling stage, a set of optimization criteria was considered according to Table S7, and the software suggested the optimal sample (namely, Opt.PH). The actual levels of the factors in this specimen comprised *A*: 9.5 wt/v %, *B*: 4 wt/v %, and *C*: 17.5 cm, and the total desirability was predicted to be 87 %. Higher desirability values indicate more probable conformity between the predictions and the actual results. In this regard, after the electrospinning of the Opt.PH, the actual responses were measured (Y_1: 211 nm, Y_2: 1.24, and Y_3: 0) and compared with predicted ones. Fig. 5 (a) reveals that the results had an excellent resemblance to the predictions. Moreover, the dependency of partial desirability to the simultaneous variation of only two factors has been clarified in Fig. 5 (b, **c**, and **d**). As shown, the partial desirability had a dual trend while changing the concentration of the polymeric components. This behavior demonstrates that the final DoE responses become dramatically unfavorable when the factors slightly deviate from their optimum level.

In the following, the validity of the optimized results was investigated based on the chain entanglement density, the calculations of

(a) Responses	Optimized values	
	Predicted	Actual
Y_1: Fibers mean diameter (nm)	198	211
Y_2: Fibers diameter distribution	1.32	1.24
Y_3: Defect number	0	0

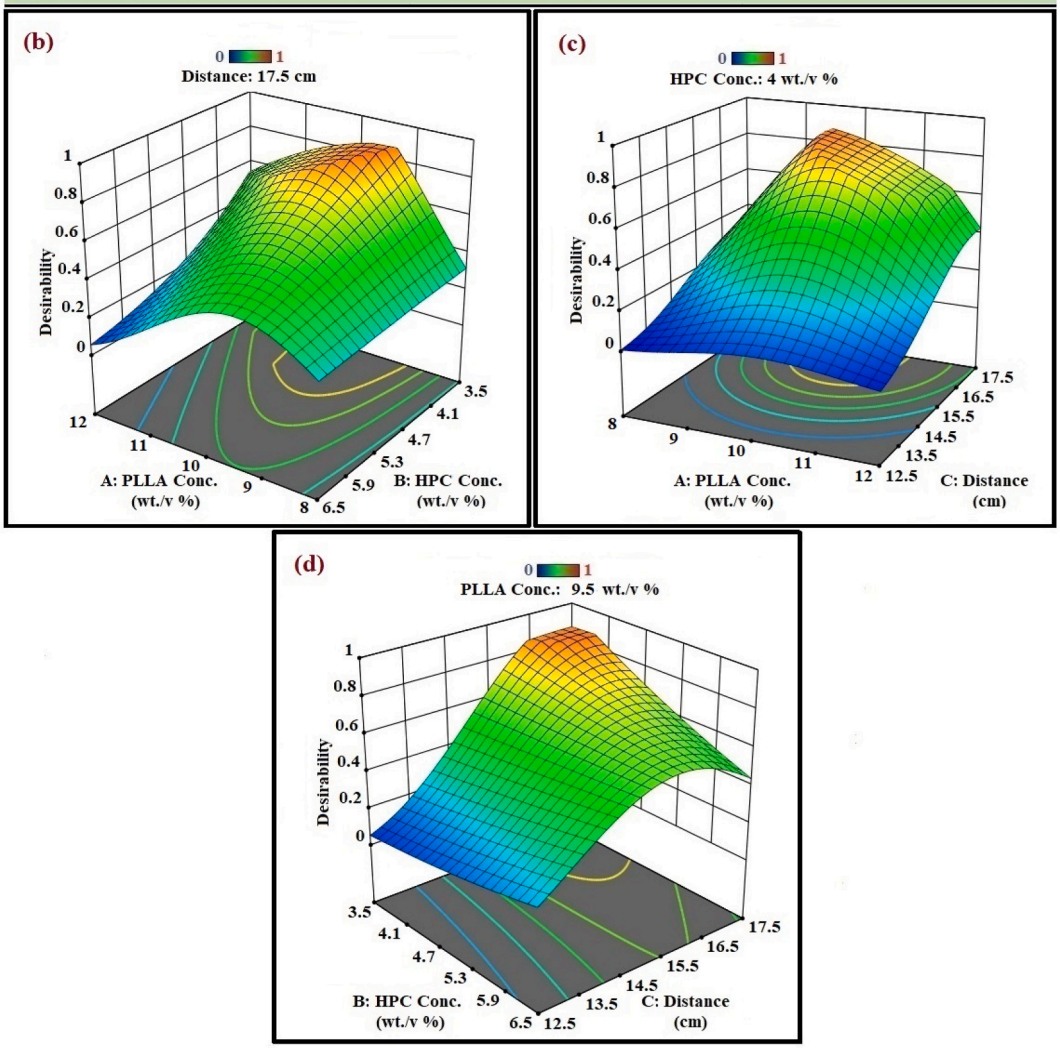

Fig. 5. (a) The suggested levels of the factors for the optimal sample (Opt.PH) and the predicted/actual values of the responses; **(b)**, **(c)**, and **(d)** the partial desirability diagrams denoting the effect of simultaneous variation of PLLA-HPC concentration, distance-PLLA concentration, and distance-HPC concentration, respectively.

which are mentioned in the Supplementary Materials. Concerning the evaluations, it could be authenticated that the optimal sample could reach a $\beta \geq 3.5$ ($\beta = 3.62$), denoting an accurate optimization.

3.2. Analysis of the morphology and viscosity/electrical conductivity

Based on the SEM images of Opt.PH and PHM samples, no bead or droplet spraying could be recognized within the fibers (Fig. 6 (a), and higher magnifications in Fig. S3). However, as shown in Fig. 6 (a), some ultrafine nanofibers were visible in Opt.PH mat, reflecting a slight jet splitting while electrospinning. This phenomenon is often attributed to incomplete mixing, unbalanced process conditions (e.g., a very high voltage) or phase separation within the solution [17]. Since the mixing/electrospinning process was carefully controlled, the appearance of this anomaly should be followed up in the solution structure. It is believed that imperfect miscibility of the polymeric components may lead to phase separation and, subsequently, to jet splitting. So, though a visually single-phase solution of PLLA/HPC could be obtained using the novel solvents (CF:DMF), there were seemingly a few local phase separations in the

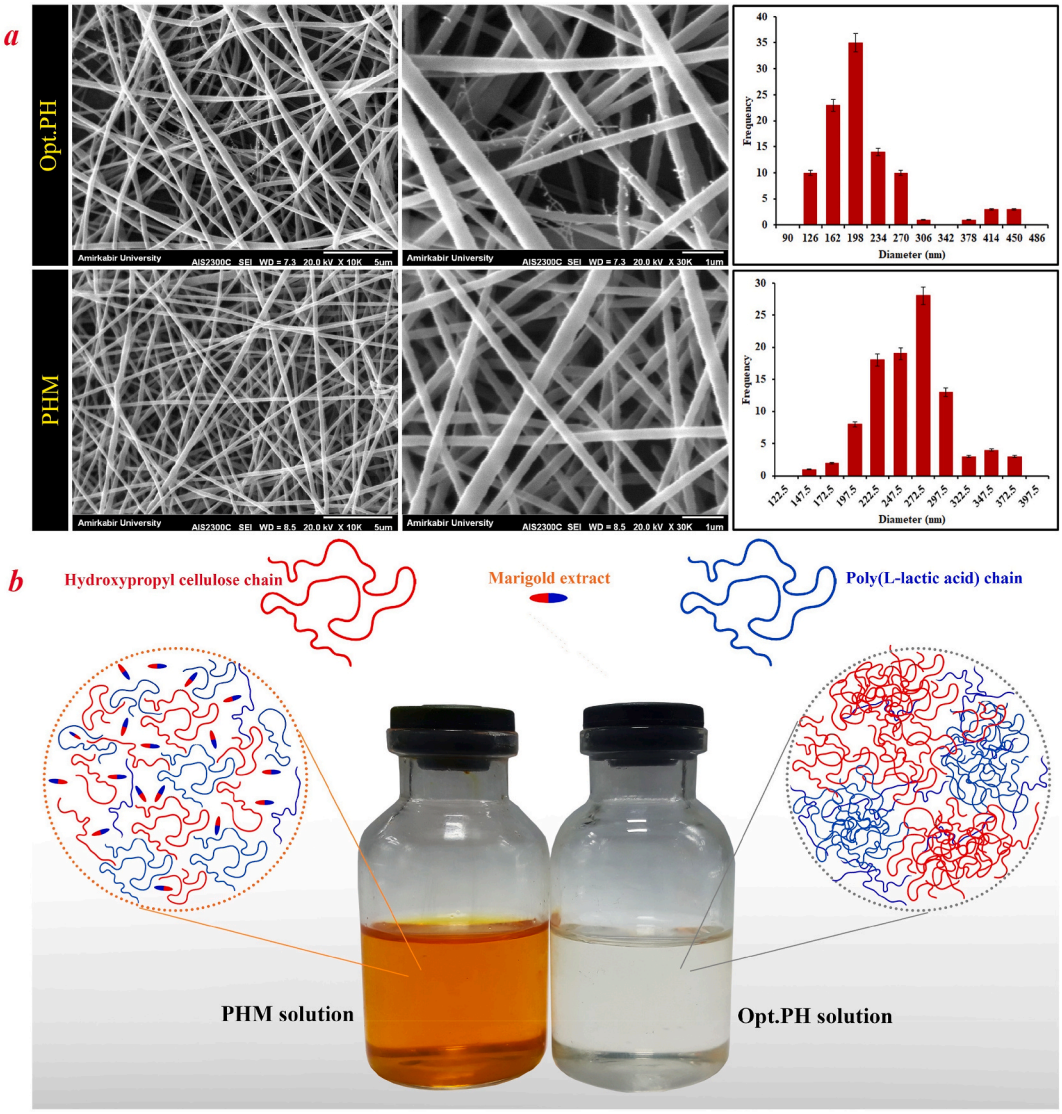

Fig. 6. (a) The SEM micrographs (in two magnifications of 1 and 5 μm), the fibers diameter distribution, and the solution schematic related to Opt. PH and PHM samples; **(b)** schematic of local and micro-scale phase separation in Opt.PH and PHM.

Table 1
The morphology, viscosity and conductivity characterization of Opt.PH and PHM solutions/mats.

Sample	Viscosity (cp)	Conductivity (μS/cm)	Average fiber diameter (nm)	Average pore size (nm)	Porosity percentage (%)
Opt.PH	120 ± 26	18.7 ± 0.5	211 ± 28	425 ± 217	73.5 ± 4.9
PHM	208 ± 15	19.1 ± 1.07	262 ± 34	483 ± 102	81.0 ± 7.3

microstructure of the solution. All these while that the addition of *Marigold* extract to PHM caused the removal of ultrafine nanofibers. This behavior may liaise with the simultaneous existence of polar and non-polar components in this extract, which reduces the thermodynamic disfavor between the non-polar (PLLA) and polar (HPC) polymeric chains (Fig. 6 (b)). Notably, conducting a higher thermodynamic tendency makes the chains leave their coil state and become more extended, preventing the jet from splitting during electrospinning. In a distinct research, Kharat et al. also declared that the presence of 3 % *Marigold* slightly enhanced the conductivity of a polymeric solution based on chitosan/polyethylene oxide and could ameliorate the uniformity of the ultimate electrospun fibers [30].

To bring more clarification regarding the effect of *Marigold* on the miscibility of components as well as the morphology of the fibers, viscosity and electrical conductivity of Opt.PH and PHM were measured in the solution state. According to Table 1, although both

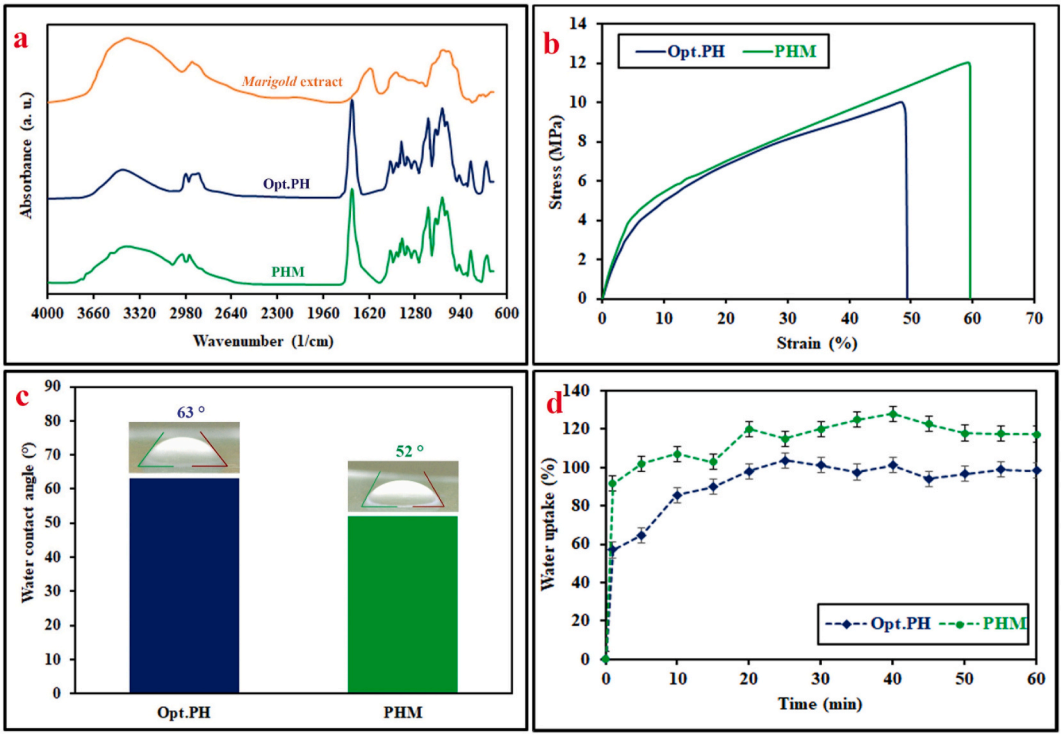

Fig. 7. (a) The ATR-FTIR spectrum of the Marigold extract, Opt.PH and PHM; **(b)** The stress-strain diagrams of the Opt.PH and PHM samples; **(c)** WCA analysis of the Opt.PH and PHM; The water uptake behavior related to the Opt.PH and PHM.

Table 2
The assigned ATR-FTIR peak bands of Opt.PH and PHM mats.

Assignment to the chemical group	Wavenumber (cm^{-1})
Amorphous phase	765
stretching of crystalline phase $-C-C-$	861
Rocking mode of $-CH_3$	926 and 964
Stretching of $-C-O-$	1061, 1093, and 1140
Bending of $-C=O$ (carbonyl)	1190
Stretching of $-C-O-$	1226
Bending of $-CH-$	1300–1342
Asymmetric and symmetric deformation $-CH-$	1383 and 1431
Bending of $-CH_3$ (methyl)	1472
Stretching of $-C=O$ (carbonyl)	1730

solutions had nearly similar electrical conductivity, PHM reached a higher viscosity level, confirming the above-mentioned content. Additionally, the average fiber diameter, average pore size, and surface porosity in this mat were in higher records. The appropriate justification should be pursued in the fundamentals of electrospinning. In such a process, the viscosity increment reduces the driving forces and, subsequently, the jet stretching during flight time. This phenomenon increases the average fiber diameter and, as a rule of thumb, is associated with the elevation of average pore size and surface porosity in the final mat [36].

3.3. Chemical identification via the ATR-FTIR spectroscopy

The ATR-FTIR spectra of the *Marigold* extract, Opt.PH, and PHM samples are given in Fig. 7 (a). In the spectrum of the *Marigold*, the peaks located at the wavenumber of 1656, 1465, 1250, and 1053 cm^{-1} are ascribed to amide I, antisymmetric band of methyl, ether groups, and terpenoids or flavones compounds, respectively. Also, the peaks at 3428 cm^{-1}, present in all the plots, are assigned to the hydroxyl group existent in HPC/*Marigold* structure. Likewise, the peak corresponding to the symmetric/asymmetric stretching of the $-CH_2$ in all samples (and alkyl in *Marigold*) is observed at 2948 cm^{-1} [31,40].

As shown, the spectra of Opt.PH and PHM mats are significantly similar, illustrating the addition of marigold extract to the Opt.PH could not lead to a chemical reaction and the formation of undesired chemical groups. However, according to the PHM spectrum, it is evident that the presence of the extract caused an increase in the intensity of the hydroxyl group peak. This phenomenon indicates the

Table 3
Comparative results of the mechanical properties reported by other researchers.

Polymeric components	Additives/agents	Properties	Application	Reference
PLLA	Curcumin	TS[a]: 3.21 ± 0.19 MPa YM[b]: 110.89 ± 8.08 MPa EB[c]: 48.68 ± 0.75 %	Skin tissue	[41]
PLLA	Dopamine Nano-silica	TS: 5.54 ± 0.35 MPa YM: 64.17 ± 0.23 MPa EB: 65 %	Bone tissue	[42]
PLLA Chitosan	–	YM: 78.67 ± 14.15 MPa EB: 77.73 ± 16.42 %	Cardiac tissue	[43]
PLLA Chitosan	Heparin	TS: 117.18 ± 7.0 MPa YM: 2.8 ± 0.2 MPa	Vascular tissue	[44]
PLLA Chitosan Collagen	–	TS: 3.19 MPa BP[d]: 1374 mmHg	Vascular tissue	[45]
PLLA poly(butylene succinate)	Cellulose nano-fibrils	TS: 3.46 ± 0.28 MPa YM: 119.6 ± 3.2 MPa EB: 115.6 ± 2.5 %	Vascular tissue	[46]
PLLA Gelatin	Doxorubicin	TS: 7.7 ± 1.3 MPa YM: 13.6 ± 1.1 MPa EB: 94 ± 5 %	- Drug delivery - General cell growth	[47]
PLDLLA PAA	–	TS: 12.7 ± 0.7 MPa YM: 5.3 ± 0.1 MPa EB: 420 ± 25 %	General cell growth	[4]
Present work				
PLLA HPC	- *Calendula oil* extract	TS: 12.1 ± 1.5 MPa YM: 95.3 ± 1.8 MPa EB: 59.6 ± 2.6 %	- Drug delivery - General cell growth	–

[a] Tensile Strength.
[b] Young Modulus.
[c] Elongation at the Break.
[d] Burst Pressure.

creation of a strong hydrogen bonding between the polymeric matrix and the *Marigold*. Such intermolecular interaction seems highly influential as it is believed to make phase separation between the PLLA and HPC weaker and slower. The rest of the characteristic peaks within the spectra of Opt.PH and PHM are given in Table 2.

3.4. Mechanical properties determination

The ideal electrospun mats, alluring for biomedical applications, should be associated with good mechanical properties until they can mimic the behavior of the desired natural tissue. According to the stress-strain diagram of the mats, PHM demonstrated a tensile strength of 12.1 ± 1.5 MPa, a Young modulus of 95.3 ± 1.8 MPa, and an elongation at the break of 59.6 ± 2.6 % (Fig. 7 (b)). These quantities touched higher levels than those in Opt.PH (tensile strength: 10.0 ± 1.8 MPa, Young modulus: 68.7 ± 4.0 MPa, and elongation at the break: 49.3 ± 3.1 %). This difference may be ascribed to the local microscale phase separation that occurred in Opt. PH and caused a different strain rate, or in other words, encountered the whole sample with a deficiency of load transfer. In this condition, the specimen would undergo the stress concentration, leading to a decrease in strength, modulus, and elongation at the break. All these are while that hydrogen bondings and *Marigold*'s stabilizing effect could boost the load transfer capability and mechanical properties (i.e., strength and modulus) of PHM. Additionally, this extract, encompassing low molecular components, acted as a plasticizer and enhanced the mobility of the polymeric chains. This feature seemingly increased the elongation at the break and facilitated stress-induced crystallization at high extensions.

In general, according to a comparative view, it is acknowledged that the mechanical properties reported in the present research are within the range of values stated in similar pieces of research (Table 3). Therefore, neglecting the local micro-scale phase separation, both Opt.PH and PHM seem qualified regarding the mechanical requirements for tissue engineering applications.

3.5. Hydrophilicity measurements

In successful scaffolds and wound dressings, achieving a hydrophilic nature is considered one of the crucial prerequisites to promote cell adhesion/spreading and cell viability/proliferation considerably. It is also clear that the hydrophilic products may be associated with significant water uptake, which is critical, especially for wound dressings. In this work, it was observed that the Opt.PH and PHM demonstrated WCAs of 63.7 ± 2.1 and 52.3 ± 1.9°, respectively. Likewise, the ultimate water uptake percentages obtained for these specimens were 98.4 ± 5.1 and 117.4 ± 3.3 %, respectively (Fig. 7 (c)). Interestingly, Kharat et al. showed that the presence of Marigold in an electrospun mat based on chitosan/polyethylene oxide could similarly reduce the WCA from 39.2 to 29.2° that, subsequently, resulted in a 70 % increase in the water uptake [30].

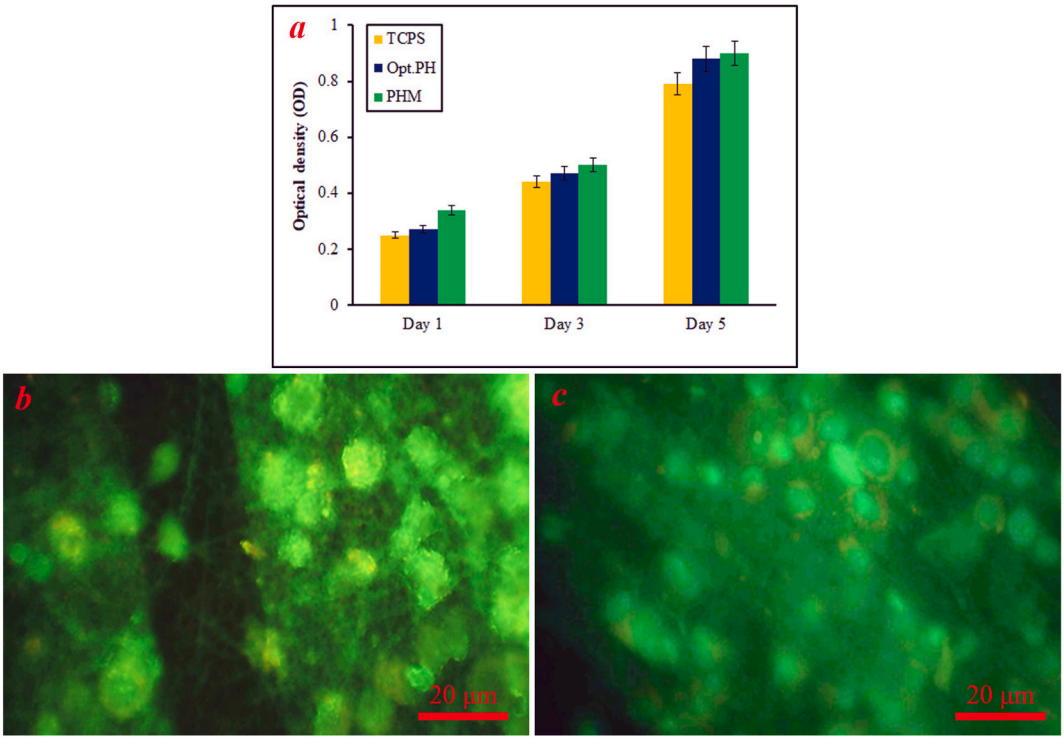

Fig. 8. (a) The bar charts of the MTT analysis denoting the cell viability of TCPS, Opt.PH, and PHM groups after 1, 3, and 5 days of cell seeding; **(b, c)** The images of the AO-stained cells on the **b**: Opt.PH, and **c**: PHM samples after 24 h of culturing.

Given that PLLA is a hydrophobic polymer and its WCA is mentioned to be 134° [42], it is believed that achieving favorable contact angles in Opt.PH and PHM originates from the efficacious presence of HPC and *Marigold*. Remarkably, as the PHM could achieve wide hydrogen bondings and a higher porosity percentage, it experienced lower WCA and, inversely, higher water uptake than Opt.PH (after 60 min) (Fig. 7 (d)).

3.6. *In vitro cell viability and cell proliferation studies*

Concerning the MTT assay, Fig. 8 (a) displays the OD graph of Opt.PH, PHM, and TCPS samples as a quantitative criterion to assess cell viability. According to the results, no signs of cell toxicity were detected in any electrospun mats on days 1, 3, and 5 after cell seeding. It is also worth mentioning that due to the higher level of hydrophilicity and porosity in PHM, this sample acquired the highest cell viability compared to the rest of the groups (during all the time points). As a complementary investigation, the AO-stained fibroblast cells qualitatively showed that both Opt.PH and PHM had proper cell compatibility after 24 h of culturing (Fig. 8 (b and **c)**).

Based on the SEM image of the fibroblast cells cultured on the electrospun mats, it is evident that the ECM-mimicking ability in both Opt.PH and PHM could provide an adequate level of cell attachment (Fig. 9). However, it seems that the cell pseudopods in the Opt.PH sample have marched only in selected pathways and led to poor quality/uniformity of the overall cell spreading. This selective spreading may be due to the slightly heterogeneous structure of Opt.PH. In other words, it is believed that the microscale phase separation in this mat obliged the cells to spread only along the domains with higher hydrophilicity (i.e., a higher concentration of HPC). However, according to the SEM images, it is apparent that such restrictions do not come up in PHM. Therefore, the proliferation and distribution of cells are quite progressive in this product.

3.7. *Investigation of the drug release behavior*

The capability of PHM electrospun mat to serve as a drug delivery system was examined regarding the *in vitro* cumulative release of *Marigold* extract. According to Fig. 10 (a), it was found that *Marigold* passed its burst release within 160 min and eventually touched its plateau after 540 min with the ultimate release fraction of 0.89 ± 0.02. Due to the anti-inflammatory properties, this drug is justified to be applied with a high release rate. However, it is authenticated that the addition of some retarding mechanisms may allow the release to be controlled and sustained. In the present work, in line with the release mechanism/kinetic characterization, cumulative data were fitted in eight models according to Fig. 10 (b-i).

It is clear that the Kopcha-Alfrey, Korsmeyer-Peppas, Baker-Lonsdale, and Gompertz models concurrently had the best fit with $R^2 \geq 0.97$. Based on the Kopcha-Alfrey model, $(K_{A1}/K_{A2}) \geq 1$ denotes that the diffusion overcame the erosion while releasing the

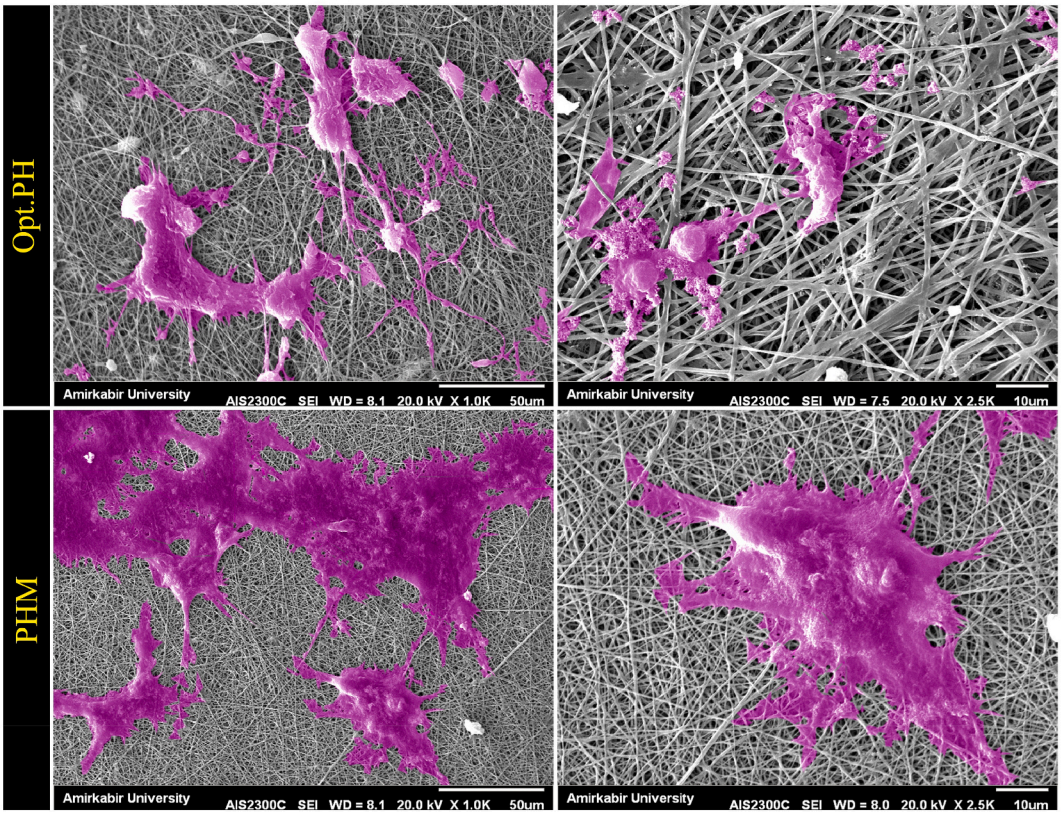

Fig. 9. SEM images of the cell cultured on the Opt.PH and PHM samples after 24 h of culturing (in two magnifications of 50 and 10 μm). The upper row and the lower row are assigned to Opt.PH and PHM samples, respectively.

Marigold. Likewise, the exponent of the Korsmeyer-Peppas model was within the range of $0.5 \leq n \leq 1$ (i.e., $n = 0.69$), which emphasizes the Non-Fickian diffusion (anomalous regime). In other words, it is supposed that the drug molecule encountered the relaxation and swelling mechanism of polymeric chains during the release procedure [48,49]. In this regard, the calculated diffusion coefficient was $D = 2.073 \times 10^{-14}$ cm^2/s. All in all, it is confirmed that *Marigold* had sufficient interaction with PLLA and HPC chains and did not tend to form local accumulation. Therefore, alongside the suitable biocompatibility of PHM, this complex would be strongly promising for further studies regarding the fabrication of fibrous drug delivery systems.

4. Conclusion

This research aspired to develop PLLA/HPC-based electrospun mats supposed to be applied in biomedical applications. The *Marigold* extract was also employed to prove the drug delivery ability of this complex. Additionally, all the designing stages followed RSM to attain optimal sample (Opt.PH). Next, a single dose of Marigold (10 mg/ml) was added (PHM sample), and both specimens were subjected to engineering and *in vitro* investigations. SEM micrographs revealed that the average fiber diameter, pore size, and porosity percentage of the PHM were 262 ± 34 nm, 483 ± 102 nm, and 81.0 ± 7.3 %, respectively, which were higher than those in Opt.PH (211 ± 28 nm, 425 ± 217 nm, 73.5 ± 4.9 %). These achievements were attributed to higher viscosity in the solution of PHM. It is also observed that the addition of *Marigold* dwindled the thermodynamic disfavor between the polymeric components and caused higher mechanical properties in PHM. In this regard, the tensile strength, Young modulus, and elongation at the break in this sample were 12.1 ± 1.5 MPa, 95.3 ± 1.8 MPa, and 59.6 ± 2.6 %, respectively. Additionally, it was ascertained that the presence of hydrogen bonding throughout the samples could result in low WCAs intensified with the addition of *Marigold*. As another result, the cumulative drug release data showed a non-Fickian diffusion while releasing the drug. Accordingly, the ultimate release fraction of 0.89 ± 0.02 could obtain after 540 min. Moreover, it was concluded that the Kopcha-Alfrey, Korsmeyer-Peppas, Baker-Lonsdale, and Gompertz had the best fit among the desired kinetic models. In this regard, the release exponent acquired by the Korsmeyer-Peppas model was $n = 0.69$, denoting an anomalous release (with the diffusion coefficient of $D = 2.073 \times 10^{-14}$ cm^2/s). Ultimately, bioassays performed on Opt.PH and PHM samples exhibited no sign of cytotoxicity and resulted in prominent cell proliferation. Based on all these results, it is verified that the electrospun mats obtained in this work can highly satisfy the initial requirements related to biomedical products and would be promising for further research.

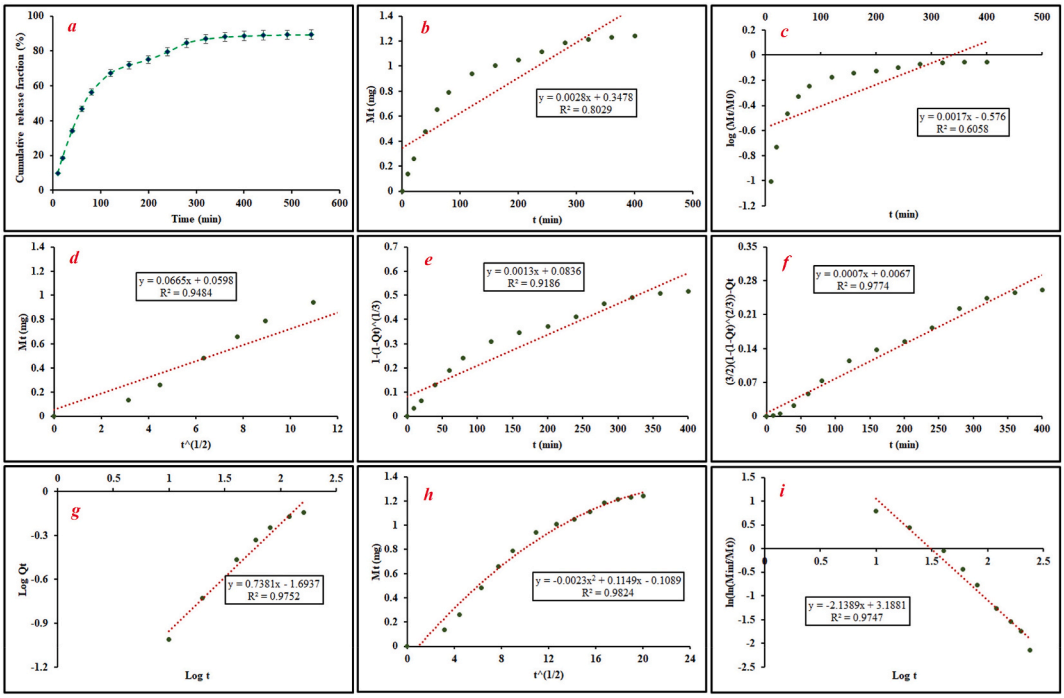

Fig. 10. (a) The plot of cumulative *Marigold* release from PHM mat; **(b–i)** The data fitted in the kinetic models of **b**: Zero-order, **c**: First-Order, **d**: Higuchi, **e**: Hixson-Crowell, **f**: Baker-Lonsdale, **g**: Korsmeyer-Peppas, **h**: Kopcha-Alfrey, **i**: Gompertz.

Formatting of funding sources

This research did not receive any specific grant from funding agencies in the public, commercial, or not-for-profit sectors.

Data availability statement

The data will be made available on request.

CRediT authorship contribution statement

Pegah Momeni: Writing - review & editing, Visualization, Validation, Methodology, Data curation, Conceptualization. **Maryam Nourisefat:** Writing - review & editing, Validation, Software, Investigation, Data curation, Conceptualization. **Arman Farzaneh:** Writing - original draft, Methodology, Investigation. **Mohammad Shahrousvand:** Supervision, Project administration, Methodology, Funding acquisition, Conceptualization. **Mohammad Hossein Abdi:** Writing - review & editing, Software, Data curation.

Declaration of competing interest

The authors declare that they have no known competing financial interests or personal relationships that could have appeared to influence the work reported in this paper.

Appendix A. Supplementary data

Supplementary data to this article can be found online at https://doi.org/10.1016/j.heliyon.2023.e23218.

References

[1] M. Rahmati, D.K. Mills, A.M. Urbanska, M.R. Saeb, J.R. Venugopal, S. Ramakrishna, M. Mozafari, Electrospinning for tissue engineering applications, Prog. Mater. Sci. 117 (2021), 100721, https://doi.org/10.1016/j.pmatsci.2020.100721.

[2] T.Y. Huang, M. Shahrousvand, Y.T. Hsu, W.T. Su, Polycaprolactone/Polyethylene glycol blended with dipsacus asper wall extract nanofibers promote osteogenic differentiation of periodontal ligament stem cells, Polymers 13 (2021), https://doi.org/10.3390/polym13142245.

[3] P. Ghaffari-Bohlouli, F. Hamidzadeh, P. Zahedi, M. Shahrousvand, M. Fallah-Darrehchi, Antibacterial nanofibers based on poly(l-lactide-co-d, l-lactide) and poly (vinyl alcohol) used in wound dressings potentially: a comparison between hybrid and blend properties, J. Biomater. Sci. Polym. Ed. 31 (2020) 219–243, https://doi.org/10.1080/09205063.2019.1683265.

[4] P. Ghaffari-Bohlouli, M. Shahrousvand, P. Zahedi, M. Shahrousvand, Performance evaluation of poly (L-lactide-co-D, L-lactide)/poly (acrylic acid) blends and their nanofibers for tissue engineering applications, Int. J. Biol. Macromol. 122 (2019) 1008–1016, https://doi.org/10.1016/j.ijbiomac.2018.09.046.

[5] H. Gharib Khajeh, M. Sabzi, S. Ramezani, A.A. Jalili, M. Ghorbani, Fabrication of a wound dressing mat based on Polyurethane/Polyacrylic acid containing Poloxamer for skin tissue engineering, Colloids Surfaces A Physicochem. Eng. Asp. 633 (2022), 127891, https://doi.org/10.1016/j.colsurfa.2021.127891.

[6] Y. Yue, X. Gong, W. Jiao, Y. Li, X. Yin, Y. Si, J. Yu, B. Ding, In-situ electrospinning of thymol-loaded polyurethane fibrous membranes for waterproof, breathable, and antibacterial wound dressing application, J. Colloid Interface Sci. 592 (2021) 310–318, https://doi.org/10.1016/j.jcis.2021.02.048.

[7] M. Shahrousvand, M. Hajikhani, L. Nazari, A. Aghelinejad, M. Shahrousvand, M. Irani, A. Rostami, Preparation of colloidal nanoparticles PVA-PHEMA from hydrolysis of copolymers of PVAc-PHEMA as anticancer drug carriers, Nanotechnology 33 (2022), 275603, https://doi.org/10.1088/1361-6528/ac6089.

[8] M.A. Ketabi, M. Shanavazi, R. Fekrazad, F. Tondnevis, Electrospun poly caprolactone-carbon nanotube scaffold for Nerve regeneration in dental tissue engineering, Int. Clin. Neurosci. J. 3 (2016) 144–149.

[9] A.D. Juncos Bombin, N.J. Dunne, H.O. McCarthy, Electrospinning of natural polymers for the production of nanofibres for wound healing applications, Mater. Sci. Eng. C. 114 (2020), 110994, https://doi.org/10.1016/j.msec.2020.110994.

[10] R. Gobi, P. Ravichandiran, R.S. Babu, D.J. Yoo, Biopolymer and synthetic polymer-based nanocomposites in wound dressing applications: a review, Polymers 13 (2021), https://doi.org/10.3390/polym13121962.

[11] M. Shahrousvand, F.A. Tabar, E. Shahrousvand, A. Babaei, M.M. Hasani-Sadrabadi, G.M.M. Sadeghi, H. Jafari, A. Salimi, High aspect ratio phospho-calcified rock candy-like cellulose nanowhiskers of wastepaper applicable in osteogenic differentiation of hMSCs, Carbohydr. Polym. 175 (2017) 293–302, https://doi.org/10.1016/j.carbpol.2017.08.001.

[12] D. Park, K. Ahn, S. Maity, T. Bhuyan, J. Yang, R. Jin, Adsorption , and controlled release of doxorubicin from cellulose acetate/polyurethane/multi-walled carbon nanotubes composite nano fi bers, (n.d.). https://doi.org/10.1088/1361-6528/ac467b.

[13] T. Yang Nilsson, M. Andersson Trojer, A solution blown superporous nonwoven hydrogel based on hydroxypropyl cellulose, Soft Matter 16 (2020) 6850–6861, https://doi.org/10.1039/d0sm00724b.

[14] H. Seddiqi, E. Oliaei, H. Honarkar, J. Jin, L.C. Geonzon, R.G. Bacabac, J. Klein-Nulend, Cellulose and its Derivatives: towards Biomedical Applications, Springer Netherlands, 2021, https://doi.org/10.1007/s10570-020-03674-w.

[15] M.H. El-Newehy, M.E. El-Naggar, S. Alotaiby, H. El-Hamshary, M. Moydeen, S. Al-Deyab, Green electrospining of hydroxypropyl cellulose nanofibres for drug delivery applications, J. Nanosci. Nanotechnol. 18 (2017) 805–814, https://doi.org/10.1166/jnn.2018.13852.

[16] K. Wulf, D. Arbeiter, C. Matschegewski, M. Teske, J. Huling, K.P. Schmitz, N. Grabow, S. Kohse, Smart releasing electrospun nanofibers - poly: L.lactide fibers as dual drug delivery system for biomedical application, Biomed. Mater. 16 (2021), https://doi.org/10.1088/1748-605X/abbec8.

[17] S. Rashedi, S. Afshar, A. Rostami, M. Ghazalian, H. Nazockdast, Co-electrospun poly(lactic acid)/gelatin nanofibrous scaffold prepared by a new solvent system: morphological, mechanical and in vitro degradability properties, Int. J. Polym. Mater. Polym. Biomater. 70 (2021) 545–553, https://doi.org/10.1080/00914037.2020.1740987.

[18] M.A. Ruz-Cruz, P.J. Herrera-Franco, E.A. Flores-Johnson, M.V. Moreno-Chulim, L.M. Galera-Manzano, A. Valadez-González, Thermal and mechanical properties of PLA-based multiscale cellulosic biocomposites, J. Mater. Res. Technol. 18 (2022) 485–495, https://doi.org/10.1016/j.jmrt.2022.02.072.

[19] B.W. Chieng, N.A. Ibrahim, W.M.Z.W. Yunus, M.Z. Hussein, Poly(lactic acid)/poly(ethylene glycol) polymer nanocomposites: effects of graphene nanoplatelets, Polymers 6 (2014) 93–104, https://doi.org/10.3390/polym6010093.

[20] J. Yuan, J. Shen, I.-K. Kang, Fabrication of protein-doped PLA composite nanofibrous scaffolds for tissue engineering, Polym. Int. 57 (2008) 1188–1193, https://doi.org/10.1002/pi.2463.

[21] P. Tipduangta, P. Belton, L. Fábián, L.Y. Wang, H. Tang, M. Eddleston, S. Qi, Electrospun polymer blend nanofibers for tunable drug delivery: the role of transformative phase separation on controlling the release rate, Mol. Pharm. 13 (2016) 25–39, https://doi.org/10.1021/acs.molpharmaceut.5b00359.

[22] J.F. Kim, J.H. Kim, Y.M. Lee, E. Drioli, Thermally induced phase separation and electrospinning methods for emerging membrane applications: a review, AIChE J. 62 (2016) 461–490, https://doi.org/10.1002/aic.15076.

[23] E. Rezabeigi, M. Sta, M. Swain, J. McDonald, N.R. Demarquette, R.A.L. Drew, P.M. Wood-Adams, Electrospinning of porous polylactic acid fibers during nonsolvent induced phase separation, J. Appl. Polym. Sci. 134 (2017) 1–8, https://doi.org/10.1002/app.44862.

[24] W. Huang, M.J. Wang, C.L. Liu, J. You, S.C. Chen, Y.Z. Wang, Y. Liu, Phase separation in electrospun nanofibers controlled by crystallization induced self-assembly, J. Mater. Chem. A. 2 (2014) 8416–8424, https://doi.org/10.1039/c4ta00417e.

[25] A. Leonés, L. Peponi, J.M. García-Martínez, E.P. Collar, Compositional influence on the morphology and thermal properties of woven non-woven mats of PLA/OLA/MgO electrospun fibers, Polymers 14 (2022), https://doi.org/10.3390/polym14102092.

[26] S. Zenoozi, G.M.M. Sadeghi, M. Shahrousvand, M. Rafiee, Preparation and optimization of polyurethane/crosslinked poly acrylic acid semi-IPNs containing multi wall carbon nanotube applicable for artificial tendon, Colloids Surfaces A Physicochem. Eng. Asp. 640 (2022), 128415, https://doi.org/10.1016/j.colsurfa.2022.128415.

[27] S. Jadbabaei, M. Kolahdoozan, F. Naeimi, H. Ebadi-Dehaghani, Preparation and characterization of sodium alginate-PVA polymeric scaffolds by electrospinning method for skin tissue engineering applications, RSC Adv. 11 (2021) 30674–30688, https://doi.org/10.1039/d1ra04176b.

[28] S.F.C. Guerreiro, J.F.A. Valente, J.R. Dias, N. Alves, Box-behnken design a key tool to achieve optimized PCL/gelatin electrospun mesh, Macromol. Mater. Eng. 306 (2021) 1–9, https://doi.org/10.1002/mame.202000678.

[29] A. Behravesh, M. Shahrousvand, A. Goudarzi, Poly(acrylic acid)/gum Arabic/ZnO semi-IPN hydrogels: synthesis, characterization and their optimizations by response surface methodology, Iran, Polym. J. (English Ed. 30 (2021) 655–674, https://doi.org/10.1007/s13726-021-00920-1.

[30] Z. Kharat, M. Amiri Goushki, N. Sarvian, S. Asad, M.M. Dehghan, M. Kabiri, Chitosan/PEO nanofibers containing Calendula officinalis extract: preparation, characterization, in vitro and in vivo evaluation for wound healing applications, Int. J. Pharm. 609 (2021), 121132, https://doi.org/10.1016/j.ijpharm.2021.121132.

[31] Z. Pedram Rad, J. Mokhtari, M. Abbasi, Preparation and characterization of Calendula officinalis-loaded PCL/gum Arabic nanocomposite scaffolds for wound healing applications, Iran, Polym. J. (English Ed. 28 (2019) 51–63, https://doi.org/10.1007/s13726-018-0674-x.

[32] Bhargab Deka, Bedanta Bhattacharjee, Anshul Shakya, Md Abu, Ashif Ikbal, Chayanika Goswami, Santa Sarma, Mechanism of action of wound healing activity of Calendula officinalis: a comprehensive review, Pharm. Biosci. J. 9 (2021) 28–44, https://doi.org/10.20510/ukjpb/9/i1/1609684673.

[33] S.L. Shenoy, W.D. Bates, H.L. Frisch, G.E. Wnek, Role of chain entanglements on fiber formation during electrospinning of polymer solutions: good solvent, non-specific polymer-polymer interaction limit, Polymer (Guildf). 46 (2005) 3372–3384, https://doi.org/10.1016/j.polymer.2005.03.011.

[34] R. Casasola, N.L. Thomas, S. Georgiadou, Electrospinning of poly(lactic acid): theoretical approach for the solvent selection to produce defect-free nanofibers, J. Polym. Sci., Part B: Polym. Phys. 54 (2016) 1483–1498, https://doi.org/10.1002/polb.24042.

[35] M. Doostan, M. Doostan, H. Maleki, R. Faridi Majidi, F. Bagheri, H. Ghanbari, Co-electrospun poly(vinyl alcohol)/poly(ε-caprolactone) nanofiber scaffolds containing coffee and Calendula officinalis extracts for wound healing applications, J. Bioact. Compat Polym. 37 (2022) 437–452, https://doi.org/10.1177/08839115221126714.

[36] M. Shahrousvand, N. Golshan Ebrahimi, Designing nanofibrous poly (ε -caprolactone)/hydroxypropyl cellulose/zinc oxide/Melilotus Officinalis wound dressings using response surface methodology, Int. J. Pharm. 629 (2022), 122338, https://doi.org/10.1016/j.ijpharm.2022.122338.

[37] M.I. Hassan, L.H. Chong, N. Sultana, Wettability and water uptake properties of PLA and PCL/Gelatin-based electrospun fibers, ARPN J. Eng. Appl. Sci. 11 (2016) 13604–13607.

[38] M. Shahrousvand, V. Haddadi-Asl, M. Shahrousvand, Step-by-step design of poly (ε-caprolactone)/chitosan/Melilotus officinalis extract electrospun nanofibers for wound dressing applications, Int. J. Biol. Macromol. 180 (2021) 36–50, https://doi.org/10.1016/j.ijbiomac.2021.03.046.

[39] N. Işıklan, Ü.H. Erol, Design and evaluation of temperature-responsive chitosan/hydroxypropyl cellulose blend nanospheres for sustainable flurbiprofen release, Int. J. Biol. Macromol. 159 (2020) 751–762, https://doi.org/10.1016/j.ijbiomac.2020.05.071.
[40] E.A. Ozturk, Z.R. Ege, S. Murat, G. Erdemir, S. Kuruca, Z.E. Erkmen, O. Duygulu, O. Gunduz, T. Caykara, M.S. Eroglu, Poly(L-lactic acid)/poly(ethylene oxide) based composite electrospun fibers loaded with magnesium-aluminum layered double hydroxide nanoparticles, Int. J. Biol. Macromol. 217 (2022) 562–571, https://doi.org/10.1016/j.ijbiomac.2022.07.055.
[41] P. Pankongadisak, S. Sangklin, P. Chuysinuan, O. Suwantong, P. Supaphol, The use of electrospun curcumin-loaded poly(L-lactic acid) fiber mats as wound dressing materials, J. Drug Deliv. Sci. Technol. 53 (2019), 101121, https://doi.org/10.1016/j.jddst.2019.06.018.
[42] Z. Lu, W. Wang, J. Zhang, P. Bártolo, H. Gong, J. Li, Electrospun highly porous poly(L-lactic acid)-dopamine-SiO2 fibrous membrane for bone regeneration, Mater. Sci. Eng. C. 117 (2020), 111359, https://doi.org/10.1016/j.msec.2020.111359.
[43] Y. Liu, S. Wang, R. Zhang, Composite poly(lactic acid)/chitosan nanofibrous scaffolds for cardiac tissue engineering, Int. J. Biol. Macromol. 103 (2017) 1130–1137, https://doi.org/10.1016/j.ijbiomac.2017.05.101.
[44] T. Wang, X. Ji, L. Jin, Z. Feng, J. Wu, J. Zheng, H. Wang, Z.W. Xu, L. Guo, N. He, Fabrication and characterization of heparin-grafted poly- L -lactic acid-chitosan core-shell nanofibers scaffold for vascular gasket, ACS Appl. Mater. Interfaces 5 (2013) 3757–3763, https://doi.org/10.1021/am400369c.
[45] I.A. Fiqrianti, P. Widiyanti, M.A. Manaf, C.Y. Savira, N.R. Cahyani, F.R. Bella, Poly-L-Lactic acid (PLLA)-chitosan-collagen electrospun tube for vascular graft application, J. Funct. Biomater. 9 (2018), https://doi.org/10.3390/jfb9020032.
[46] T. Abudula, U. Saeed, A. Memic, K. Gauthaman, M.A. Hussain, H. Al-Turaif, Electrospun cellulose Nano fibril reinforced PLA/PBS composite scaffold for vascular tissue engineering, J. Polym. Res. 26 (2019), https://doi.org/10.1007/s10965-019-1772-y.
[47] B. Liu, Z. Jin, H. Chen, L. Liang, Y. Li, G. Wang, J. Zhang, T. Xu, Electrospun poly (L-lactic acid)/gelatine membranes loaded with doxorubicin for effective suppression of glioblastoma cell growth in vitro and in vivo, Regen. Biomater. 8 (2021) 1–12, https://doi.org/10.1093/rb/rbab043.
[48] Y. Fu, W.J. Kao, Drug release kinetics and transport mechanisms of non-degradable and degradable polymeric delivery systems, Expert Opin. Drug Deliv. 7 (2010) 429–444, https://doi.org/10.1517/17425241003602259.
[49] M. Shahrousvand, N.G. Ebrahimi, H. Oliaie, M. Heydari, M. Mir, M. Shahrousvand, Polymeric transdermal drug delivery systems, in: Model. Control Drug Deliv. Syst., Elsevier, 2021, pp. 45–65, https://doi.org/10.1016/B978-0-12-821185-4.00017-8.